

Article

Microstructure and Tensile Properties of ECAPed Mg-9Al-1Si-1SiC Composites: The Influence of Initial Microstructures

Shaoxiong Zhang ¹, Ming Li ^{1,2}, Hongxia Wang ^{1,*}, Weili Cheng ^{1,*}, Weiwei Lei ¹, Yiming Liu ¹ and Wei Liang ¹

¹ Shanxi Key Laboratory of Advanced Magnesium-Based Materials, College of Materials Science and Engineering, Taiyuan University of Technology, Taiyuan 030024, China; zhangshaoxiong0175@link.tyut.edu.cn (S.Z.); liming9131217@163.com (M.L.); lww1836@126.com (W.L.); liuym812@163.com (Y.L.); liangwei@TYUT.edu.cn (W.L.)

² Southwest Technique and Engineering Research Institute, Chongqing 400039, China

* Correspondence: wanghongxia1217@163.com (H.W.); chengweili7@126.com (W.C.); Tel.: +86-351-601-0021

Received: 10 December 2017; Accepted: 11 January 2018; Published: 15 January 2018

Abstract: Mg-9Al-1Si-1SiC composites with various initial microstructures prior to equal channel angular pressing (ECAP) were obtained by different pre-treatments (without and with homogenization treatment), and the resultant grain size, second phase and tensile properties of ECAPed composites were reported. The ECAPed composite with homogenization treatment (HT) exhibited finer grain size, higher fraction of dynamically recrystallized (DRXed) grains, weaker texture intensity, as well as the presence of dynamic precipitated Mg₁₇Al₁₂ phase compared to that without HT. Besides, the morphology of pre-existing Mg₂Si changed from massive-like to needle-like in the ECAPed composite with HT. Room-temperature tensile test results showed that ultimate tensile strength (UTS), yield strength (YS), and elongation (El) of ECAPed composites with HT were 16.1%, 23%, and 27.3% larger than that without HT, respectively.

Keywords: Mg-9Al-1Si-1SiC composite; homogenization treatment; ECAP; microstructure; mechanical properties

1. Introduction

Due to high strength, corrosion resistance at room temperature, Mg-9%Al-1%Zn (AZ91) has been used as the most common and cost-effective commercial Mg alloy [1,2]. Unfortunately, massive secondary phases of Mg₁₇Al₁₂ in the form of coarse network structure deteriorate the strength at elevated temperature [3,4]. It has been reported that Si alloying in Mg-Al based alloys could improve the thermal stability; however, the existence of Chinese script-shaped Mg₂Si decreases the mechanical properties of Mg-Al-Si materials [5]. Recently, it has been reported that SiC nanoparticles (n-SiCp) addition [6] could refine the grain size of matrix in the SiCp/AZ91 nanocomposite and modify the morphology of Mg₁₇Al₁₂ phase from coarse plates to lamellar precipitates, resulting in simultaneous enhancement of strength and ductility. However, it is difficult to add nanoparticles into the matrix alloy and achieve dispersed distribution due to its large specific surface area. Semisolid stirring-assisted ultrasonic vibration [6] was used to fabricate a sample of as-cast n-SiCp/Mg-Al-Si composite. Although the mechanical properties were improved to an extent, it is inevitable that blowholes and mixtures were produced during the stirring process. To obtain refined microstructures and further improve mechanical properties, several conventional deformation processes (e.g., extrusion, rolling, and forging [7–9]) have been applied to n-SiCp-reinforced magnesium matrix composite. Previous studies [5,10] have shown that equal channel angular pressing (ECAP) could refine the grains

of n-SiCp/Mg-Al-Si composite and modify the morphology and distribution of the secondary phase $Mg_{17}Al_{12}$ and Mg_2Si in n-SiCp/Mg-Al-Si composite effectively. However, the network $Mg_{17}Al_{12}$ cannot be distributed uniformly when the as-cast n-SiCp/Mg-Al-Si composites are subject to ECAP [5]. It is necessary to find a method to eliminate the amount of coarse pre-existing $Mg_{17}Al_{12}$ phase. The homogenization treatment was applied on the AZ91 by dissolving the eutectic $Mg_{17}Al_{12}$ second phases and homogenizing solute atoms in the Mg matrix to reduce the potential sites of intercrystalline cracking and improve the workability of AZ91 [11].

According to previous reports, the homogenized and compressed composite exhibited much higher ultimate tensile strength than that of the compressed alloy without homogenization [12,13]. Similarly, Yuan et al. [14] reported that improved strength and ductility of ZK60 can be achieved by homogenization treatment prior to ECAP, which was attributed to the activated dynamic precipitation of $MgZn_2$ during the severe plastic deformation (SPD).

Even though a great deal of work has been done, the influence of initial grain size, morphology, and amount of reinforced second phase on the microstructural evolution and tensile properties of semi-solid casted Mg-9Al-1Si-1SiC composite fabricated by assisted ultrasonic vibration and processed by ECAP still need further investigation. Thus, the microstructural evolution and resultant tensile properties of Mg-9Al-1Si-1SiC composites subjected to different pre-treatments were studied in detail.

2. Experimental Procedures

2.1. Materials and ECAP Experiment

Mg-9Al-1Si alloy was melted in a crucible under a protective atmosphere of CO_2 and SF_6 . Pure Mg, Al, and Al-30% Si (wt %) master alloy were added to the melt. n-SiCp with an average size of 60 nm was used as reinforcement. The n-SiCp was pre-heated to 550 °C before adding to the melt. The Al-Si master alloy was added to the melt at 720 °C and held for 20 min, and then cooled down to 590 °C. Then, 1 wt % preheated SiC nanoparticles were quickly added into the semisolid slurry and stirred for 15 min. After that, the temperature was adjusted to 690 °C to make sure that the slurry converted into liquid state. During the process, the stirring rate was adjusted to 100 r/min. When the temperature reached 690 °C, the stirring process was stopped. At the same time, the ultrasonic probe was placed over the melt in the crucible to preheat for 15 min and then was dipped into the melt for ultrasonic treatment for 20 min. The power and frequency of the ultrasonic treatment device were 1.6 kW and 20 kHz, respectively. The purpose of ultrasonic treatment was to make the n-SiCp disperse uniformly in the matrix. When the ultrasonic process was stopped, the temperature was elevated to pouring temperature of 720 °C and held for 30 min. Then, n-SiCp/Mg-9Al-1Si magnesium matrix composite melt was poured into a preheated mold with a diameter of 40 mm and length of 115 mm. The samples were machined into 12 mm × 12 mm × 55 mm to fit the die used in the ECAP process. Homogenization treatment (HT) was carried at 420 °C for 24 h and then cooled to room temperature in warm water before ECAP.

A die with internal angle, Φ , of 90° between the two equal channels and the external curvature of the point of intersection of the two channels (Ψ) of 16° was designed for the ECAP process. The ECAP experiment was conducted at 360 °C for four passes. Route Bc [15–17] was selected and pressing speed was 2.0 mm/min. Figure 1 shows the schematic illustration of ECAP. The samples for ECAP were ground with 400, 800, and 1200 grit papers to avoid stress concentration and were scribbled with pot lead and Vaseline.

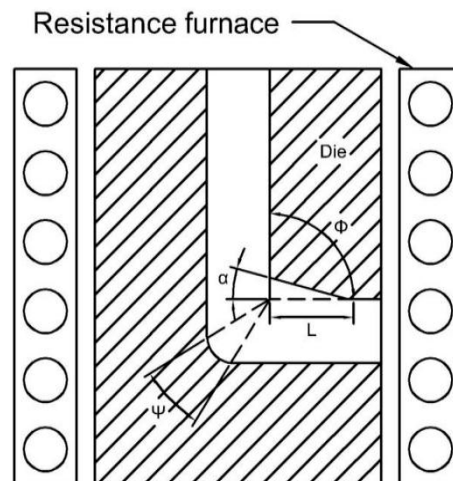


Figure 1. Schematic illustration of equal channel angular pressing (ECAP).

2.2. Microstructures and Mechanical Testing

The microstructures of the specimens were observed by a Leica 2700 M light optical microscope (LOM, Leica Microsystem GmbH, Wetzlar, Germany). The second phases of $Mg_{17}Al_{12}$ and Mg_2Si composition were determined by a MIRA3 scanning electron microscope (SEM, TESCAN Ltd., Brno-Kohoutovice, Czech Republic) equipped with an energy dispersive spectrometer (EDS). The existence of $Mg_{17}Al_{12}$ phase was certified by a JEM-2100F transmission electron microscope (TEM, JEOL Ltd., Tokyo, Japan). The average grain size, the amounts of both dynamically recrystallized (DRXed) grains and precipitates were calculated from the number and/or area fraction using at least ten micrographs by Image-Pro Plus 6.0 software (Media Cybernetics, Rockville, MD, USA). (0002) pole figures of the ECAPed samples were performed with a Y-2000 X-ray diffractometer (XRD, Cu-K α , Dandong Ray instrument Co., Ltd., Dandong, China). Samples for microstructure analysis were prepared by the conventional mechanical polishing and etching using 4.2 g picric acid, 10 mL acetic acid, 90 mL alcohol, and 10 mL distilled water. Specimens for TEM observation were prepared by grinding–polishing to produce a foil of 30 μm thickness followed by punching 3 mm diameter disks. The disks were ion beam-thinned. The tensile test was conducted in a WDW-100kN tensile machine (Jinan Test Machine Co., Ltd, Jinan, China) at room temperature, and the velocity was controlled at 0.5 mm/min. Before conducting the tensile test, the prepared samples were ground with sand paper.

3. Results and Discussions

3.1. Microstructures

In Figure 2a,c, it is apparent that as-cast Mg-9Al-1Si-1SiC composite exhibits a typical dendritic microstructure with primary α -Mg matrix, secondary γ -phase ($Mg_{17}Al_{12}$), and Chinese script-shaped phases (Mg_2Si). In addition, EDS results of secondary phases are also given in Figure 2c. It can be seen from Figure 2b,d that most of the γ -phases disappear and all the Mg_2Si phases remain after HT. According to the Mg-Al binary phase diagram, the $Mg_{17}Al_{12}$ phase has a melting point of 458 °C and the equilibrium solid solubility of Al in Mg at 420 °C is approximately 12 wt %, so few $Mg_{17}Al_{12}$ phases could remain in the composite after HT. Meanwhile, Mg_2Si phase with a higher melting point still existed in the α -Mg matrix. The different EDS results in Figure 2c,d illustrate that the disappearing secondary phases are $Mg_{17}Al_{12}$, which is in agreement with the facts. Generally, the changes of the amount of second phases have a significant effect on the various ECAP morphologies, as well as related tensile properties, which will be discussed in the following sections.

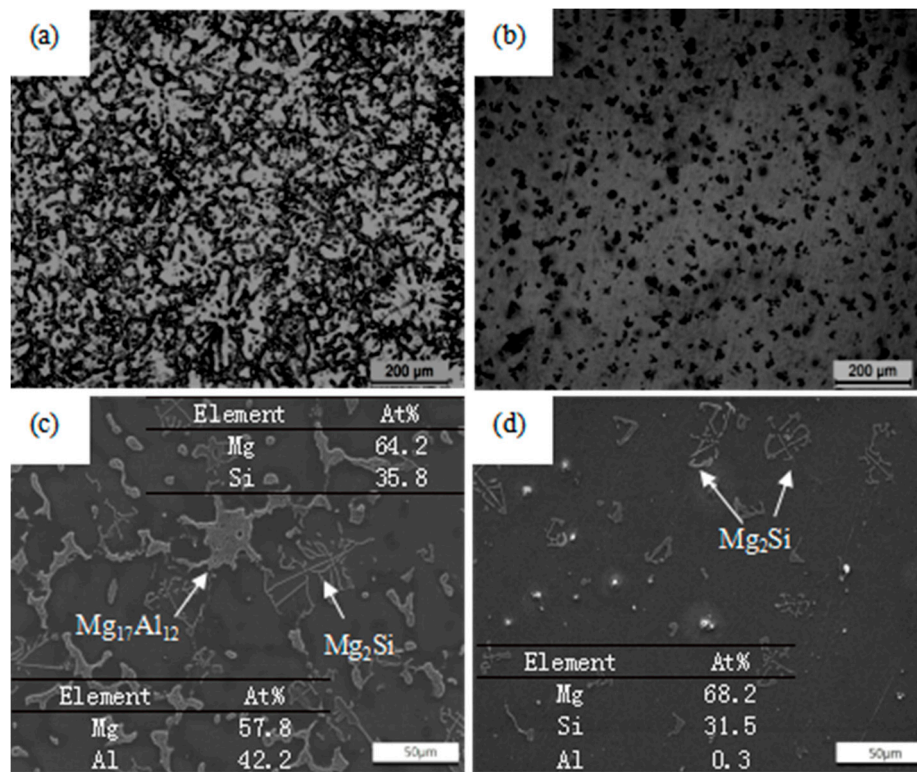


Figure 2. Optical, SEM (scanning electron microscope) micrographs, and EDS (energy dispersive spectrometer) results of Mg-9Al-1Si-1SiC composites prior to ECAP: (a,c) without HT (homogenization treatment); (b,d) with HT.

A microstructure with nearly equiaxed coarse grains is observed in Figure 3a. In addition, the measured area fraction and average size of DRXed grains (F_{DRX} and d_{DRX}) for ECAPed Mg-9Al-1Si-1SiC composite without HT were $\sim 82.8\%$ and $\sim 10.6 \mu\text{m}$ (as shown in Figure 3a), respectively. The grain size distribution is given in Figure 3b, and the average grain size of ECAPed Mg-9Al-1Si-1SiC composite without HT was $18.56 \mu\text{m}$. It can be seen from Figure 3c that ECAPed Mg-9Al-1Si-1SiC composites with HT exhibited a typical bimodal structure, which consisted of fine and equiaxed DRXed grains and coarse un-recrystallized grains. A previous study [18] reported that a bimodal structure is beneficial to the simultaneous improvement of the strength and ductility. Similarly, the measured area fraction and average size of DRXed grains (F_{DRX} and d_{DRX}) for ECAPed Mg-9Al-1Si-1SiC composite with HT were $\sim 93.4\%$ and $\sim 6.4 \mu\text{m}$ (as shown in Figure 3c). As indicated, the measured area fraction (F_{DRX}) was 12.8% larger and the average size of DRXed grains (d_{DRX}) for ECAPed Mg-9Al-1Si-1SiC composite with HT was 39.6% smaller than that without HT. The results above point to a decrease of average grain size in ECAPed Mg-9Al-1Si-1SiC composite with HT. The grain size distribution is exhibited in Figure 3d, and the average grain size of ECAPed Mg-9Al-1Si-1SiC composite with HT was 30.6% smaller than that without HT. This can be explained by the production of numerous precipitates in ECAPed Mg-9Al-1Si-1SiC composite with HT during ECAP process, which hinders the DRXed grains' growth by pinning grain boundary.

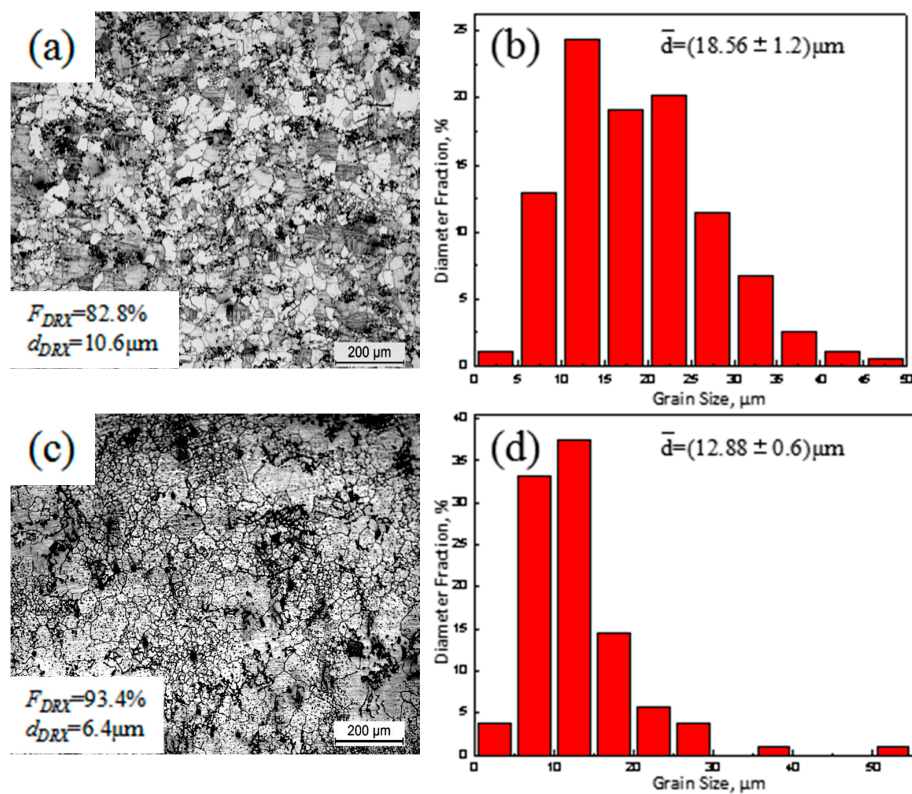


Figure 3. Optical micrographs and grain size distribution of ECAPed Mg-9Al-1Si-1SiC composites: (a,b) without HT; (c,d) with HT.

Figure 4 displays the SEM micrographs of ECAPed Mg-9Al-1Si-1SiC composites without and with HT, respectively. After ECAP, $\text{Mg}_{17}\text{Al}_{12}$ phase and Mg_2Si were both segregated into fragments (as shown in Figure 4a). The obvious agglomeration is also observed in Figure 4a, and the sizes of most $\text{Mg}_{17}\text{Al}_{12}$ particles are above $10\ \mu\text{m}$. It can be seen from Figure 4b that both $\text{Mg}_{17}\text{Al}_{12}$ precipitates and Mg_2Si phases were rearranged and uniformly distributed. In addition, the morphology of the initial Chinese script Mg_2Si changed into a needle-like morphology. Meanwhile, finer $\text{Mg}_{17}\text{Al}_{12}$ phases with size of smaller than $10\ \mu\text{m}$ precipitated through dynamic precipitation [10] in ECAPed Mg-9Al-1Si-1SiC composite with HT. The results reveals that HT contributes to a more refined and uniform microstructure.

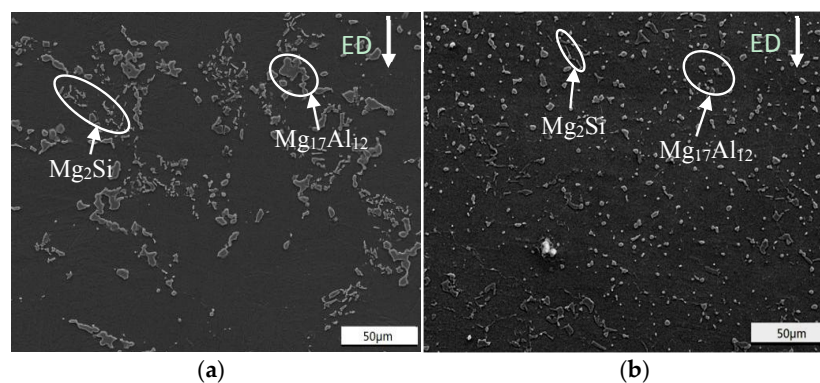


Figure 4. SEM micrographs of ECAPed Mg-9Al-1Si-1SiC composites: (a) without HT; (b) with HT. ED: extrusion direction.

The number per area of $Mg_{17}Al_{12}$ particles was larger than $1 \mu m$ in the ECAPed Mg-9Al-1Si-1SiC composite, as shown in Figure 5. As indicated, the number per area of particles ranging from $1 \mu m$ to $10 \mu m$ in size of the ECAPed composite with HT was larger than that of their counterpart without HT. It is well known that particles with size $1\sim 10 \mu m$ can act as nucleation sites for DRX during hot deformation, because of the higher dislocation density and large orientation gradient induced at the deformed zones in the vicinity of the particles [19]. This phenomenon is known as particle-stimulated nucleation (PSN), and has been widely observed in wrought Mg alloys [20,21]. For this reason, a larger amount of particles with size of $1\sim 10 \mu m$ led to a higher fraction of DRXed grains in ECAPed Mg-9Al-1Si-1SiC composites with HT.

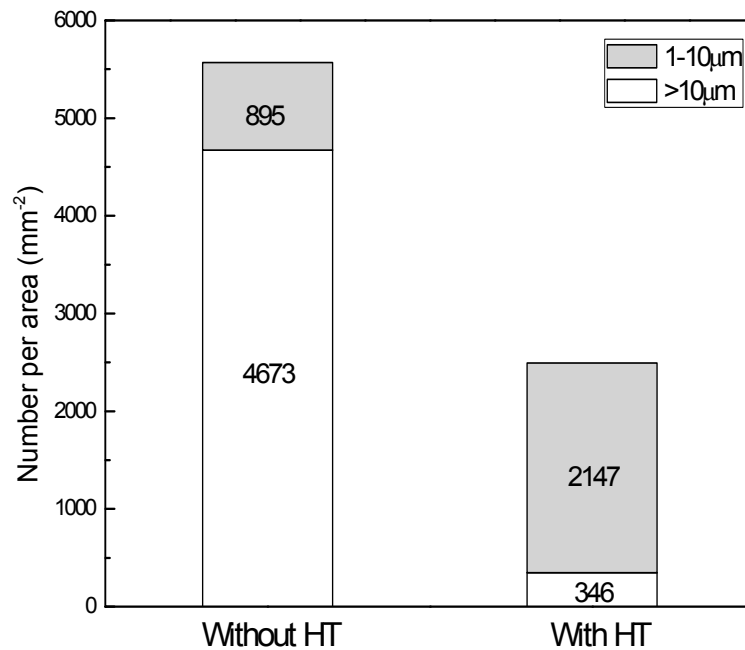


Figure 5. Particle-size distribution and number per area for ECAPed Mg-9Al-1Si-1SiC composites.

Furthermore, the existence of SiC nanoparticles has a positive effect on the uniform distribution of fine $Mg_{17}Al_{12}$ and Mg_2Si particles by pinning effect [22,23]. Therefore, the grains of ECAPed composite with HT were greatly refined.

Figure 6 shows the (0002) pole figures of ECAPed Mg-9Al-1Si-1SiC composite without HT and with HT, respectively. As indicated, the intensity of the basal texture of ECAPed Mg-9Al-1Si-1SiC composite without HT and with HT were 8.8 and 4.2, respectively. The c-axis of most grains rotated approximately 90° with respect to the extrusion direction (ED). However, some other grains tilted 30° with respect to the extrusion direction. Furthermore, a previous study [21] indicated the DRX grains form from the randomly oriented grains. Thus, a larger DRX fraction will increase the randomness of the grain orientation and finally decrease the texture intensity [24]. Besides, $Mg_{17}Al_{12}$ phases precipitated during ECAP provide more randomly oriented nuclei, and contribute to blocking the mobility of dislocations and grain boundaries. In other words, the larger the amount of dynamic precipitates, the weaker the texture of the composite. The aforementioned texture characteristics in ECAPed samples with HT will be beneficial to ductility.

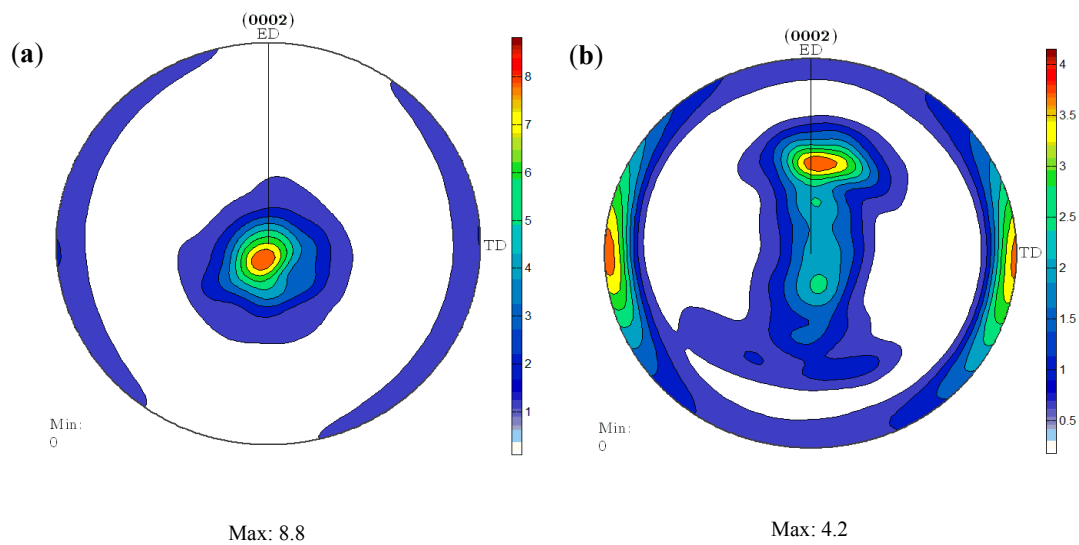


Figure 6. The (0002) pole figures of ECAPed Mg-9Al-1Si-1SiC composites: (a) without HT; (b) with HT.

3.2. Mechanical Properties

Figure 7a shows the tensile stress–strain curves of ECAPed Mg-9Al-1Si-1SiC composites without and with HT. The results show that ultimate tensile strength (UTS), yield strength (YS), and elongation (El) of the ECAPed composite with HT were 16.1%, 23%, and 27.3% larger than that of ECAPed composites without HT, respectively. The effect of HT on the mechanical properties of the ECAPed composites is remarkable. This could be attributed to the greatly refined matrix grain size and a more uniform distribution of second phases [25]. It is generally believed that the YS of wrought magnesium alloys can be associated with grain size, dynamic precipitation, and texture intensity. The YS value for metals and alloys is calculated by Hall–Petch relation [26]:

$$\sigma_y = \sigma_0 + Kd^{-1/2} \quad (1)$$

where σ_y is the YS, σ_0 is the material constant, and K is the Hall–Petch slope, with a value of $300 \text{ MPa } \mu\text{m}^{1/2}$. Increment in YS by grain refinement from $10.6 \mu\text{m}$ to $6.4 \mu\text{m}$ was about 26.4 MPa , suggesting that a decrease of DRXed grain size could partially enhance the strengthening effect. In addition, the precipitated $\text{Mg}_{17}\text{Al}_{12}$ particles during ECAP can serve as obstacles to dislocation movement based on Orowan mechanism [27,28]. In general, the precipitated small particles act as obstacles for the grain boundary migration and greatly hinder the growth of matrix grains, which results in fine grain size in the ECAPed Mg-9Al-1Si-1SiC composite with HT and make a great contribution to grain boundary strengthening. Similarly, the dislocations piled up around second phase precipitates in the ECAPed Mg-9Al-1Si-1SiC composite with HT, as observed in Figure 7b. The electron diffraction patterns of point A (as shown in Figure 7d) indicate that the phase is $\text{Mg}_{17}\text{Al}_{12}$. Thus, it can be seen that Orowan mechanism plays an important role in the improvement of mechanical properties of ECAPed Mg-9Al-1Si-1SiC composites.

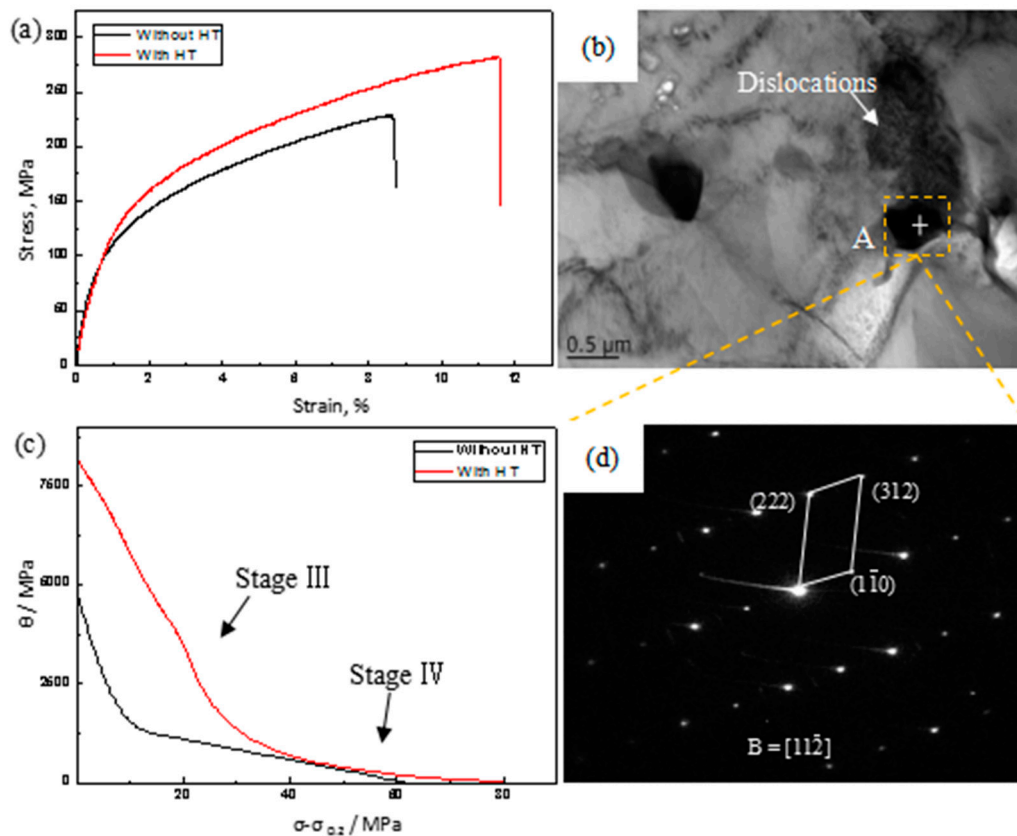


Figure 7. The tensile properties and bright-field TEM image of ECAPed Mg-9Al-1Si-1SiC composites: (a) typical tensile stress–strain curves; (b) dislocations; (c) work hardening curves; (d) selected area diffraction patterns of point A.

It is noteworthy that ECAPed Mg-9Al-1Si-1SiC composite with HT exhibited better ductility than the one without HT. Previous study has revealed that a more random texture in the extruded alloy with T4 could lead to more dislocation slip, giving rise to an increment of El [29]. Work hardening behavior of ECAPed alloys can be described by work hardening rate: $\theta = \partial\sigma/\partial\varepsilon$, where σ and ε are the true stress and true strain of the alloy, respectively. The $\sigma_{0.2}$ is subtracted from σ , and thus $\sigma - \sigma_{0.2}$ is related to the dislocation contribution to the flow stress. Figure 7c shows the work hardening rate (θ) versus net flow stress $\sigma - \sigma_{0.2}$ of ECAPed Mg-9Al-1Si-1SiC composites without and with HT. It is clearly observed that there is no initially linear hardening behavior (stage II), only a dynamic recovery stage (stage III) and a large-strain work hardening stage (stage IV) appear in the $\theta - (\sigma - \sigma_{0.2})$ curves of the present alloys [21,30,31]. Generally, stage II is related to high dislocation density. However, high dislocation density is attributed to ultrafine DRXed grains and dispersed dynamic precipitates with nanoscale size, which are not observed in our study. Therefore, stage II does not occur. Meanwhile, it can be seen from Figure 7c that the work hardening rates of ECAPed Mg-9Al-1Si-1SiC composite without and with HT demonstrated an almost linear decrease with increasing stress in stage III, but the ECAPed Mg-9Al-1Si-1SiC composite without HT dropped faster. It has been proved that the decreasing grain size is beneficial for dislocation slipping and increasing dynamic recovery rate [32]. Since the average grain size of ECAPed Mg-9Al-1Si-1SiC composite with HT is small, it can be inferred that such fine grains play an important role in the decrease of θ value at stage III. Stage IV is the large-strain work hardening stage, which refers to the formation of a dislocation cell structure [33]. In addition, the work-hardening exponents obtained from the Hollomon equation ($\sigma = K\varepsilon^n$, where K is the strength coefficient) were calculated as 0.56 and 0.78 for ECAPed Mg-9Al-1Si-1SiC composites without and with HT, respectively. It is generally

known that a large work-hardening exponent leads to a low sensitivity to strain localization, resulting in enhanced elongation.

3.3. Fracture Surface

Figure 8 shows the fracture surfaces of samples prepared from ECAPed composites without and with HT after tensile tests, respectively. Micro-cracks and dimples can be observed in Figure 8a. Dimples are also observed in Figure 8b, but the dimples are deeper than that of ECAPed samples without HT. The micro-cracks in ECAPed Mg-9Al-1Si-1SiC composite without HT explain its poor ductility. The deeper dimples and tear ridges in ECAPed Mg-9Al-1Si-1SiC composite with HT result in its better El.

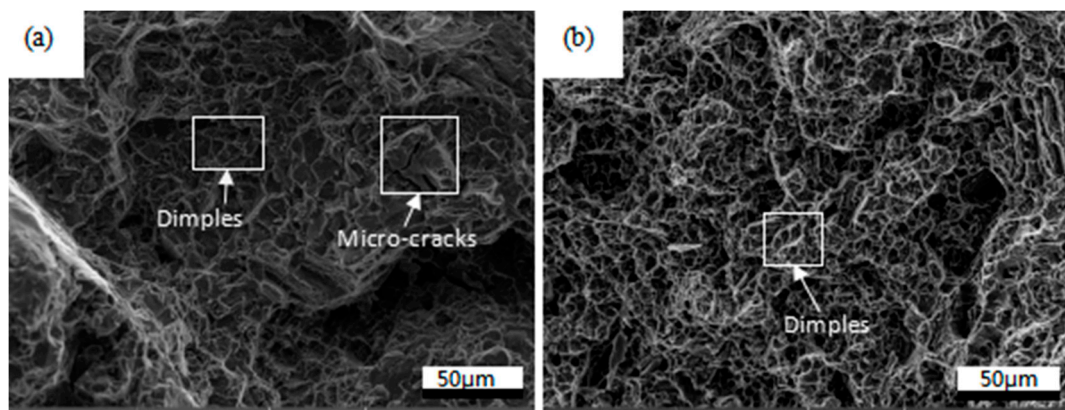


Figure 8. SEM fractography of ECAPed Mg-9Al-1Si-1SiC composites: (a) without HT; (b) with HT.

4. Conclusions

(1) Homogenization treatment prior to ECAP induces a more homogeneous and refined microstructure in terms of grain and second phases in the matrix. In addition, the texture intensity of ECAPed Mg-9Al-1Si-1SiC composite with HT decreases greatly due to the higher fraction of DRXed grains and second phase particles.

(2) The UTS, YS, and El of ECAPed composites with HT were 16.1%, 23%, and 27.3% larger than that of ECAPed composites without HT, respectively.

(3) The enhanced tensile strength and ductility in ECAPed Mg-9Al-1Si-1SiC composite with HT is attributed to the combined effects of grain boundary strengthening, precipitation strengthening and texture modification.

Acknowledgments: This work was financially supported by National Natural Science Foundation of China (51771129, 51301118, 51404166), Natural Science Foundation of Shanxi Province (201701D121045); Shanxi key laboratory of advanced magnesium-based material Taiyuan University of Technology (AMM-2017-12).

Author Contributions: Shaoxiong Zhang and Hongxia Wang conceived and designed the experiments; Shaoxiong Zhang and Ming Li performed the experiments; Shaoxiong Zhang, Weili Cheng and Weiwei Lei analyzed the data; Yiming Liu and Wei Liang contributed analysis tools, Shaoxiong Zhang wrote the paper, Hongxia Wang, Weili Cheng revised the manuscript.

Conflicts of Interest: The authors declare no conflict of interest.

References

1. Mordike, B.L.; Ebert, T. Magnesium: Properties-applications-potential. *Mater. Sci. Eng. A* **2001**, *302*, 37–45. [[CrossRef](#)]
2. Wang, X.J.; Xu, D.K.; Wu, R.Z.; Chen, X.B.; Peng, Q.M.; Jin, L.; Xin, Y.C.; Zhang, Z.Q.; Liu, Y.; Chen, X.H.; et al. What is going on in magnesium alloys? *J. Mater. Sci. Technol.* **2017**. [[CrossRef](#)]

3. Nie, K.B.; Wang, X.J.; Deng, K.K.; Xu, F.J.; Wu, K.; Zheng, M.Y. Microstructures and mechanical properties of AZ91 magnesium alloy processed by multidirectional forging under decreasing temperature Conditions. *J. Alloys Compd.* **2014**, *617*, 979–987. [[CrossRef](#)]
4. Zhang, X.H.; Cheng, Y.S. Tensile anisotropy of AZ91 magnesium alloy by equal channel angular Processing. *J. Alloys Compd.* **2015**, *622*, 1105–1109. [[CrossRef](#)]
5. Wang, W.H.; Wang, H.X.; Liu, Y.Y.; Nie, H.H.; Cheng, W.L. Effect of nanoparticles addition on the microstructures and mechanical properties of ECAPed Mg-9Al-1Si. *J. Mater. Res.* **2017**. [[CrossRef](#)]
6. Nie, K.B.; Wang, X.J.; Hu, X.S.; Xu, L.; Wu, K.; Zheng, M.Y. Microstructure and mechanical properties of SiC nanoparticles reinforced magnesium matrix composites fabricated by ultrasonic vibration. *Mater. Sci. Eng. A* **2011**, *528*, 5278–5282. [[CrossRef](#)]
7. Choi, H.; Alba-Baena, N.; Nimityongskul, S.; Jones, M.; Wood, T.; Sahoo, M.; Lakes, R.; Kou, S.; Li, X. Characterization of hot extruded Mg/SiC nanocomposites fabricated by casting. *J. Mater. Sci.* **2011**, *46*, 2991–2997. [[CrossRef](#)]
8. Khoshzaban Khosroshahi, H.; Fereshteh Saniee, F.; Abedi, H.R. Mechanical properties improvement of cast AZ80 Mg alloy/nano-particles composite via thermomechanical processing. *Mater. Sci. Eng. A* **2014**, *595*, 284–290. [[CrossRef](#)]
9. Nie, K.B.; Wang, X.J.; Xu, F.J.; Wu, K.; Zheng, M.Y. Microstructure and tensile properties of SiC nanoparticles reinforced magnesium matrix composite prepared by multidirectional forging under decreasing temperature conditions. *Mater. Sci. Eng. A* **2015**, *639*, 465–473. [[CrossRef](#)]
10. Qiao, X.G.; Ying, T.; Zheng, M.Y.; Wei, E.D.; Wu, K.; Hu, X.S.; Gan, W.M.; Brokmeier, H.G.; Golovin, I.S. Microstructure evolution and mechanical properties of nano-SiCp/AZ91 composite processed by extrusion and equal channel angular pressing (ECAP). *Mater. Charact.* **2016**, *121*, 222–230. [[CrossRef](#)]
11. Shahzad, M.; Qureshi, A.H.; Waqas, H.; Rafi, U.D. Influence of pre- and post-extrusion heat treatments on microstructure and anisotropy of mechanical properties in a Mg-Al-Zn alloy. *Mater. Des.* **2013**, *51*, 870–875. [[CrossRef](#)]
12. El Aal, M.I.A. Influence of the pre-homogenization treatment on the microstructure evolution and the mechanical properties of Al-Cu alloys processed by ECAP. *Mater. Sci. Eng. A* **2011**, *528*, 6946–6957. [[CrossRef](#)]
13. Zhang, L.; Wang, Q.D.; Liao, W.J.; Guo, W.; Ye, B.; Jiang, H.Y.; Ding, W.J. Effect of homogenization on the microstructure and mechanical properties of the repetitive-upsetting processed AZ91D alloy. *J. Mater. Sci. Technol.* **2017**, *33*, 935–940. [[CrossRef](#)]
14. Yuan, Y.C.; Ma, A.B.; Gou, X.F.; Jiang, J.H.; Arhin, G.; Song, D.; Liu, H. Effect of heat treatment and deformation temperature on the mechanical properties of ECAP processed ZK60 magnesium alloy. *Mater. Sci. Eng. A* **2016**, *677*, 125–132. [[CrossRef](#)]
15. Wan, D.Q.; Wang, J.C.; Wang, G.F.; Lin, L.; Feng, Z.G.; Yang, G.C. Precipitation and responding damping behavior of heat-treated AZ31 magnesium alloy. *Acta Metall.* **2009**, *22*, 1–6. [[CrossRef](#)]
16. Jounghsik, S.; José, V.H.; Dietmar, L.; Roland, G.; Wolfram, V. Effect of processing route on texture and cold formability of AZ31 Mg alloy sheets processed by ECAP. *Mater. Sci. Eng. A* **2016**, *669*, 159–170. [[CrossRef](#)]
17. Bleckmann, M.; Eichhorst, M.; Schuch, M.; Kreuzer, W.; Hammond, V.H.; Spiller, C.; Meyer, L.W.; Herzig, N. The influence of selected ECAP-processing routes on the material properties of Magnesium Elektron 675. *Mater. Sci. Eng. A* **2016**, *660*, 108–117. [[CrossRef](#)]
18. Park, S.H.; Kim, S.H.; Kim, Y.M.; You, B.S. Improving mechanical properties of extruded Mg-Al alloy with a bimodal grain structure through alloying addition. *J. Alloys Compd.* **2015**, *646*, 932–936. [[CrossRef](#)]
19. Kim, S.H.; Park, S.H. Influence of Ce addition and homogenization temperature on microstructural evolution and mechanical properties of extruded Mg-Sn-Al-Zn alloy. *Mater. Sci. Eng. A* **2016**, *676*, 232–240. [[CrossRef](#)]
20. She, J.; Pan, F.; Zhang, J.; Tang, A.; Luo, S.; Yu, Z.; Song, K.; Rashad, M. Microstructure and mechanical properties of Mg-Al-Sn extruded alloys. *J. Alloys Compd.* **2016**, *657*, 893–905. [[CrossRef](#)]
21. Cheng, W.L.; Tian, L.; Wang, H.X.; Bian, L.P.; Yu, H. Improved tensile properties of an equal channel angular pressed (ECAPed) Mg-8Sn-6Zn-2Al alloy by prior aging treatment. *Mater. Sci. Eng. A* **2017**, *687*, 148–154. [[CrossRef](#)]
22. Xie, C.; Wang, Y.N.; Fang, Q.H.; Ma, T.F.; Zhang, A.B.; Peng, W.F.; Shu, X.D. Effects of cooperative grain boundary sliding and migration on the particle cracking of fine-grained magnesium alloys. *J. Alloys Compd.* **2017**, *704*, 641–648. [[CrossRef](#)]

23. Ding, H.; Liu, L.; Kamado, S.; Ding, W.J.; Kojima, Y. Evolution of microstructure and texture of AZ91 alloy during hot compression. *Mater. Sci. Eng. A* **2007**, *452–453*, 503–507. [[CrossRef](#)]
24. Cheng, W.L.; Bai, Y.; Wang, L.F.; Wang, H.X.; Bian, L.P.; Yu, H. Strengthening Effect of Extruded Mg-8Sn-2Zn-2Al Alloy: Influence of Micro and Nano-Size Mg₂Sn precipitates. *Materials* **2017**, *10*, 822. [[CrossRef](#)] [[PubMed](#)]
25. Estrin, Y.; Vinogradov, A. Extreme grain refinement by severe plastic deformation: A wealth of challenging science. *Acta Mater.* **2013**, *61*, 782–817. [[CrossRef](#)]
26. Cheng, W.L.; Tian, Q.W.; Yu, H.; Zhang, H.; You, B.S. Strengthening mechanisms of indirect-extruded Mg-Sn based alloys at room temperature. *J. Magnes. Alloys* **2014**, *2*, 299–304. [[CrossRef](#)]
27. Kang, J.W.; Sun, X.F.; Deng, K.K.; Xu, F.J.; Zhang, X.; Bai, Y. High strength Mg-9Al serial alloy processed by slow extrusion. *Mater. Sci. Eng. A* **2017**, *697*, 211–216. [[CrossRef](#)]
28. Ma, K.; Wen, H.; Hu, T.; Topping, T.D.; Isheim, D.; Seidman, D.N.; Lavernia, E.J. Mechanical behavior and strengthening mechanisms in ultrafine grain precipitation-strengthened aluminum. *Acta Mater.* **2014**, *62*, 144–155. [[CrossRef](#)]
29. Such, B.C.; Kim, J.H.; Bae, J.H.; Hwang, J.H.; Shim, M.S.; Kima, N.J. Effect of Sn addition on the microstructure and deformation behavior of Mg-3Al alloy. *Acta Mater.* **2017**, *124*, 268–279. [[CrossRef](#)]
30. Kang, J.W.; Wang, C.J.; Deng, K.K.; Nie, K.B.; Bai, Y.; Li, W.J. Microstructure and mechanical properties of Mg-4Zn-0.5Ca alloy fabricated by the combination of forging, homogenization and extrusion process. *J. Alloys Compd.* **2017**, *720*, 196–206. [[CrossRef](#)]
31. Li, W.J.; Deng, K.K.; Zhang, X.; Wang, C.J.; Kang, J.W.; Nie, K.B.; Liang, W. Microstructures, tensile properties and work hardening behavior of SiCp/Mg-Zn-Ca composites. *J. Alloys Compd.* **2017**, *695*, 2215–2223. [[CrossRef](#)]
32. Del Valle, J.A.; Carreño, F.; Ruano, O.A. Influence of texture and grain size on work hardening and ductility in magnesium-based alloys processed by ECAP and rolling. *Acta Mater.* **2006**, *54*, 4247–4259. [[CrossRef](#)]
33. Ungár, T.; Zehetbauer, R.M. Stage IV work hardening in cell forming materials, part II: A new mechanism. *Scr. Mater.* **1996**, *35*, 1467–1473. [[CrossRef](#)]



© 2018 by the authors. Licensee MDPI, Basel, Switzerland. This article is an open access article distributed under the terms and conditions of the Creative Commons Attribution (CC BY) license (<http://creativecommons.org/licenses/by/4.0/>).